

Perspective

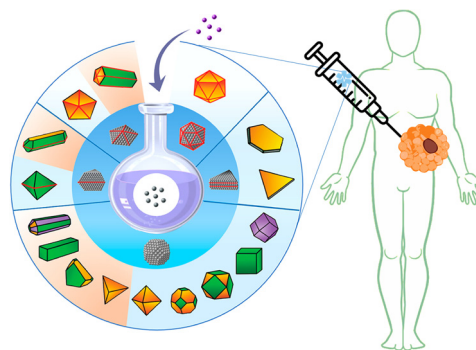
Noble-Metal Nanocrystals: From Synthesis to Biomedical Applications

Yidan Chen¹, Emily Yan², and Younan Xia^{2,*}¹ School of Materials Science and Engineering, Georgia Institute of Technology, Atlanta, GA 30332, USA² Wallace H. Coulter Department of Biomedical Engineering, Georgia Institute of Technology and Emory University, Atlanta, GA 30332, USA

* Correspondence: younan.xia@bme.gatech.edu

Received: 24 February 2025; Accepted: 26 February 2025; Published: 28 February 2025

Abstract: Noble metals hold promises for a variety of biomedical applications due to their unique physical and biochemical properties. To unlock this potential, a significant amount of research has been dedicated to the controlled synthesis of noble-metal nanocrystals over the past two decades, with a particular emphasis on the production of Au and Ag nanocrystals with diverse and well-controlled shapes. The successful synthesis of noble-metal nanocrystals with tunable sizes, shapes, and morphologies allows researchers to explore their use in a range of biomedical applications, including contrast enhancement for an array of bioimaging modalities, facilitating stimuli-responsive drug delivery, and functioning as antimicrobial or anticancer agents.



Keywords: noble metals; nanocrystal synthesis; biomedical applications

1. Introduction

Noble metals refer to ruthenium (Ru), rhodium (Rh), palladium (Pd), osmium (Os), iridium (Ir), platinum (Pt), and gold (Au). They are considered “noble” due to their resistance to corrosion and thus natural occurrence in the elemental form. Sometimes, silver (Ag), copper (Cu), and mercury (Hg) are also included as noble metals, albeit these elements typically occur in nature as sulfides. Noble metals have found widespread use in catalysis, electronics, photonics, and plasmonics. The increasingly efficient synthesis of noble-metal nanocrystals also renders new opportunities in a spectrum of biomedical applications [1], including sensing, imaging, diagnostics, controlled release, targeted drug delivery, advanced therapy, and antimicrobial coating. As a major advantage over other types of materials, the surface of noble-metal nanocrystals can be robustly modified with organic ligands to increase their biocompatibility, alter their biodistribution in vivo, and/or entail additional functionalities, such as targeting specific biomarkers overexpressed on the surface of malignant cells.

When used as nanocrystals, their properties and thus figures of merit in various applications can be tuned by optimizing their size, shape, and morphology or by varying the composition in the case of an alloy [1]. For nanocrystals based on Au, Ag, and Cu, they possess remarkable optical properties due to their ability to efficiently absorb and scatter light in the visible and near-infrared (NIR) regions, enabling applications in the context of localized surface plasmon resonance (LSPR) and surface-enhanced Raman spectroscopy (SERS). LSPR refers to the collective oscillation of conductive-band electrons upon excitation by light, whereas SERS enhances the sensitivity of Raman spectroscopy by leveraging the enhancement of local electric field to amplify the Raman scattering cross-section of molecules near the surface of nanocrystals. Both LSPR and SERS have facilitated the development of advanced biosensing techniques and imaging modalities, enhancing our ability to detect biomarkers and resolve malignant tissues.

Noble-metal nanocrystals have also shown promise in theranostics, a research theme that aims to integrate diagnosis with therapy. In theranostics, nanocrystals can serve as both imaging and therapeutic agents, making it feasible to simultaneously visualize and eradicate malignant cells. One such imaging modality is photoacoustic



Copyright: © 2025 by the authors. This is an open access article under the terms and conditions of the Creative Commons Attribution (CC BY) license (<https://creativecommons.org/licenses/by/4.0/>).

Publisher's Note: Scilight stays neutral with regard to jurisdictional claims in published maps and institutional affiliations.

tomography (PAT), which relies on optical absorption to generate ultrasound signals upon excitation by a pulsed laser. The exceptional absorption capability of Au-based nanocrystals positions them as a class of superior contrast agents for PAT [2]. In parallel, Au-based nanocrystals have been extensively explored as photothermal transducers for localized hyperthermia treatment. In this case, the heat derived from photothermal conversion can be used to destroy malignant cells and pathogens at the diseased site without affecting the surrounding healthy tissues. Position emission tomography (PET) is a non-invasive modality that relies on the positrons emitted from a radioactive isotope (e.g., ^{64}Cu) to produce gamma rays when they interact with tissues, allowing for the monitoring of physiological activities and measurement of changes in metabolic processes. To this end, Au-Cu alloy nanocrystals can be directly utilized as a radioactive tracer for PET when some of the ^{63}Cu atoms are substituted with ^{64}Cu .

2. Colloidal Synthesis of Noble-Metal Nanocrystals

Solution-phase synthesis is the most versatile and robust route for producing noble-metal nanocrystals (Figure 1a) [3]. The synthesis typically starts with the generation of metal atoms through the chemical reduction or thermal decomposition of a salt precursor. The concentration of the atoms continues to increase until it reaches the threshold for homogeneous nucleation. At this point, the atoms aggregate to generate small clusters, commonly referred to as nuclei, followed by their growth and evolution into seeds with well-defined internal structures [3,4]. For noble metals, the seeds generally adopt one of the following four internal structures: single-crystal, singly-twinned, multiply-twinned, and stacking-fault-lined [4]. The internal structure, in conjunction with kinetic and thermodynamic factors during the subsequent growth step, ultimately determines the shape taken by the nanocrystals. In general, one needs to optimize the precursor, reducing agent, capping agent, and stabilizer (including both the type and concentration) to obtain nanocrystals uniform in terms of both shape and size. Over the past decades, extensive research has been conducted to elucidate the mechanistic details involved in solution-phase syntheses and the protocols for reproducibly producing nanocrystals with controlled shapes, with a focus on those made of Au, Ag, Cu, Pd, Pt, and their alloys. Readers should consult the most recent literature to find the updated protocols.

Polycrystalline Au nanoparticles (AuNPs) with a quasi-spherical shape can be conventionally prepared by reducing HAuCl_4 in a solution phase (Figure 1b) [2]. Two of the established protocols were originally developed by Turkevich and Brust, respectively. In the Turkevich method, HAuCl_4 is reduced with sodium citrate in water at an elevated temperature (e.g., 100 °C). The size of the resulting AuNPs is mainly determined by the molar ratio between the reactants. A study by Peng and coworkers demonstrated that relatively uniform particles with sizes in the range of 20–40 nm could be obtained using this simple method [5]. As for the Brust method, it entails transferring the HAuCl_4 precursor into an organic solvent such as toluene and controlling the growth of the AuNPs with a thiol-based capping agent (e.g., 1-dodecanethiol) to obtain particles below 10 nm in size [2].

Unlike the quasi-spherical nanoparticles, Au nanospheres (AuNSs) can be made with a single-crystal structure while assuming a spherical shape that gives a circular projection under transmission electron microscopy (Figure 1c) [2]. To this end, our group developed a facile route for synthesizing AuNSs by utilizing Au clusters capped with hexadecyltrimethylammonium bromide (CTAB) as the initial seeds for a repeated growth process [6,7]. In a typical protocol, the initial seeds are mixed with a precursor such as HAuCl_4 , a capping agent based on hexadecyltrimethylammonium chloride (CTAC), and a reductant such as ascorbic acid (AA) in water at room temperature. Through meticulous control of the reaction conditions, uniform AuNSs with tunable diameters in the range of 5–150 nm were consistently produced [6,7].

Another popular class of Au nanocrystals is nanorods (NRs), characterized by a distinctive anisotropic structure (Figure 1d). Among the various methods developed for AuNR synthesis, seed-mediated growth stands out due to its simplicity in procedure, readily tunable aspect ratio for the product, and high yield of NRs with a narrow size distribution. While specific chemicals and protocols may differ among various methods of seed-mediated growth, they typically involve two stages: the initial preparation of citrate-capped Au seeds by reducing HAuCl_4 precursor with a strong reductant such as NaBH_4 in water, followed by their introduction into a growth medium [8]. The growth medium usually consists of the precursor, a surface capping agent (e.g., CTAB) to stabilize the colloid and initiate/guide the anisotropic growth, and a moderately strong reductant such as AA [8]. To increase the uniformity and purity of the products, it is critical to introduce AgNO_3 or an aromatic additive like 5-bromosalicylic acid or 2,6-dihydroxybenzoic acid [2].

Characterized by their well-defined sharp corners, Ag nanocubes (Figure 1e) have received increasing attention in recent years for their applications in both LSPR and SERS [9]. Our group pioneered the one-pot polyol synthesis of Ag nanocubes by employing ethylene glycol (EG) as both the solvent and reductant [10]. Subsequently,

improved protocols were developed to yield large volumes of uniform Ag nanocubes with edge lengths up to 250 nm by switching the precursor from the commonly used AgNO_3 to CF_3COOAg [11], introducing a trace amount of Na_2S or NaHS to manipulate initial nucleation [12], and/or selectively removing the twinned seeds through the use of O_2/Cl^- (NaCl or KCl) to initiate oxidative etching [13].

As a more cost-effective alternative to Au and Ag nanocrystals due to the high abundance of Cu in Earth's crust [14], Cu nanocubes (Figure 1f) also exhibit tunable LSPR in the visible and NIR regions. The colloidal synthesis of Cu nanocubes is comparatively more challenging than that of Au and Ag nanocrystals due to the lower reduction potential of Cu and greater susceptibility to oxidation. In addition to one-pot methods, seed-mediated growth has been developed as a viable route for producing Cu nanocubes with controllable sizes. In one study, for example, 5-nm AuNSs were utilized as seeds to synthesize Au@Cu core-shell nanocubes with a uniform edge length tunable from 20–30 nm. The presence of the Au seeds effectively lowered the activation energy barrier to nucleation while increasing the conversion of the CuCl_2 precursor [15].

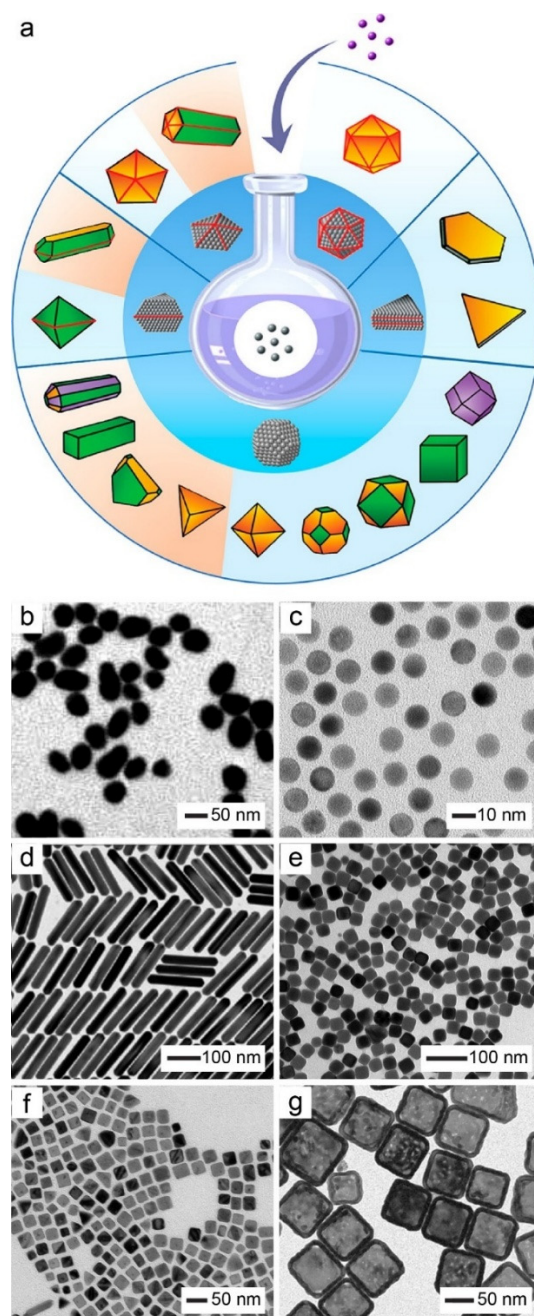


Figure 1. Colloidal synthesis of noble-metal nanocrystals. (a) Schematic showing the generation of nanocrystals with diverse and controllable shapes. (b–g) TEM images of various types of noble-metal nanocrystals: (b) Au nanoparticles; (c) Au nanospheres; (d) Au nanorods; (e) Ag nanocubes; (f) Au@Cu core-shell nanocubes; and (g) Au nanocages. (a) Reproduced with permission from [3]. Copyright 2023 Americal Chemical Society. (b) Reproduced with permission from [5]. Copyright 2007 Americal Chemical Society. (c) Reproduced with

permission from [7]. Copyright 2013 Wiley-VCH. (d) Reproduced with permission from [16]. Copyright 2015 American Chemical Society. (e) Reproduced with permission from [9]. Copyright 2013 American Chemical Society. (f) Reproduced with permission from [15]. Copyright 2019 American Chemical Society. (g) Reproduced with permission from [17]. Copyright 2019 Wiley-VCH.

Gold nanocages (AuNCs) represent a class of hollow nanocrystals characterized by ultrathin and porous walls, which are composed of either pure Au or Au-based alloys [18]. The pores in the walls can be engineered to create an “open or close” gating mechanism, allowing for controlled, on-demand release of a payload. The primary method for generating AuNCs involves the galvanic replacement reaction between Ag nanocubes and HAuCl₄ in water, a spontaneous reaction driven by the more positive standard reduction potential of AuCl₄⁻/Au (1.00 V) relative to that of Ag⁺/Ag (0.80 V). One can conveniently produce AuNCs by titrating aqueous HAuCl₄ into an aqueous mixture containing Ag nanocubes and poly(vinyl pyrrolidone) (PVP). As Ag atoms are gradually oxidized and dissolved, Au atoms are formed and deposited on the surface of the nanocubes to generate AuNCs. When Ag nanocubes with sharp corners are used, the initial oxidation and dissolution of Ag occur on the side faces to generate small pinholes, which then act as anodes for further oxidation and dissolution. Meanwhile, the resultant Au atoms are conformally deposited on the side faces. As the reaction proceeds, the pinholes are closed due to atomic diffusion and direct Au deposition, leading to the formation of Au–Ag alloy nanoboxes. Subsequent removal of Ag from the walls through a dealloying process generates AuNCs with porous walls (Figure 1g). The size, shape, and wall thickness of the AuNCs can all be tailored by changing the Ag templates, introducing a proper surface capping agent (e.g., PVP), and varying the amount of HAuCl₄. As such, one can increase the diversity of AuNCs and enhance their optical and photothermal properties. When applied to *in vivo* studies, the size and shape of the AuNCs impact both their biodistribution and therapeutic efficiency.

3. Examples of Applications

Noble metals have been employed as therapeutic agents since ancient times. Recent studies of their distinctive physical and biochemical attributes, in conjunction with advancements in controlling their colloidal synthesis (as illustrated in Section 2), have reignited interest in employing their nanocrystals for a range of biomedical applications. Notable examples include their use as antimicrobial agents and as active components in diagnostics and cancer treatment.

Due to its wide accessibility and rapid responsiveness, point-of-care (POC) diagnosis holds increasing significance in the modern healthcare industry. When conjugated with ligands targeting specific analytes, AuNPs have found extensive use in POC diagnosis, spanning infectious virus detection, diabetes monitoring, pregnancy tests, cardiovascular disease assessment, and cancer screening [19]. Enabled by their unique LSPR properties, AuNPs can be detected using a variety of methods, including colorimetric, fluorescence, and SERS. For instance, commercial pregnancy tests use AuNPs conjugated with antibodies of hCG, a hormone excreted during early pregnancy [20], to create a red test line for the indication of a positive result (Figure 2a) [21]. Similarly, during the COVID-19 pandemic, AuNP-based molecular diagnostic kits were developed to enable rapid and cost-effective screening of infected individuals [22]. In this case, instead of antibodies, the AuNPs were functionalized with antisense oligonucleotides (ASOs) to target the N-gene of SARS-CoV-2, the virus responsible for the pandemic. The agglomeration of ASO-capped AuNPs in the presence of SARS-CoV-2 triggers a discernible color change from purple to blue, which can be easily observed by the naked eye (Figure 2b).

The LSPR properties of Au nanostructures have also been put to work for other biomedical applications. Researchers have demonstrated that the LSPR peaks of Au nanostructures could be precisely tuned to cover the entire visible and NIR regions by varying their sizes and morphologies, with the latter being particularly effective [18]. For instance, a remarkable redshift of the LSPR peaks was observed for AuNRs as their aspect ratios were increased while maintaining a constant width (Figure 3a) [23]. Similarly, AuNCs exhibited precisely tunable LSPR peaks into the NIR region when the wall thickness was adjusted by controlling the degree of galvanic replacement reaction (Figure 3b) [2]. Of particular importance for biomedical applications are Au nanostructures with LSPR peaks in the window of 650–900 nm, where water, blood, and soft tissues exhibit optical transparency, facilitating deep penetration for effective imaging and treatment [18].

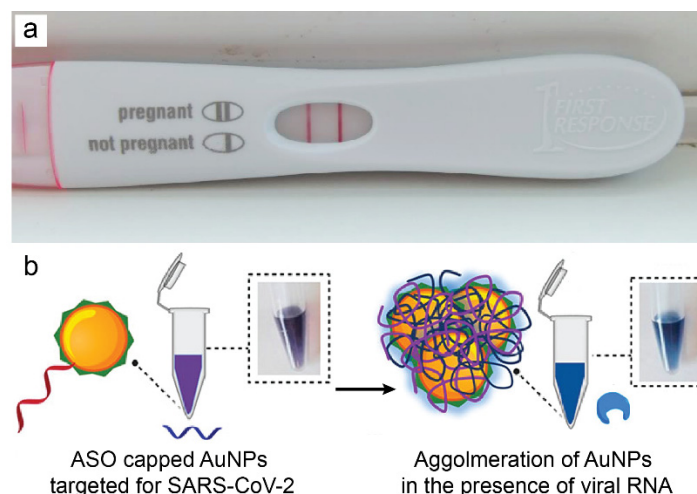


Figure 2. Use of Au nanoparticles as a colorant for point-of-care diagnosis. (a) Formation of red test lines in a commercial pregnancy test kit through the accumulation of Au nanoparticles. (b) Color change in a solution detectable by the naked eye due to the agglomeration of Au nanoparticles in the presence of SARS-CoV-2 RNA. (a) Adapted from [21]. (b) Reproduced with permission from [22]. Copyright 2020 American Science Society.

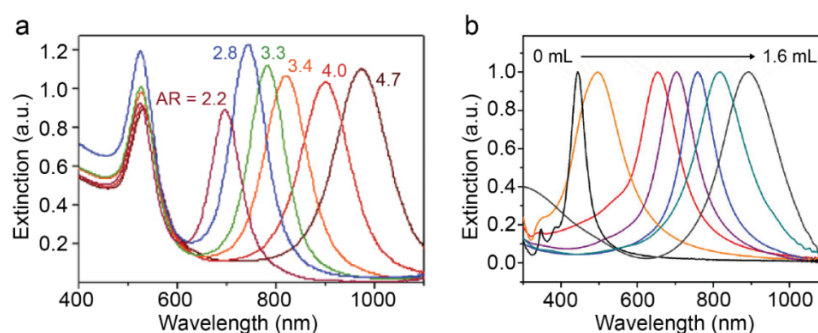


Figure 3. Tunable LSPR property of Au nanocrystals. The UV-vis-NIR spectra were recorded from aqueous suspensions of (a) Au nanorods with different aspect ratios (ARs) and (b) Au nanocages prepared by titrating different amounts of HAuCl₄ (volume = 0–1.6 mL). (a) Reproduced with permission from [24]. Copyright 2006 the Royal Society of Chemistry. (b) Reproduced with permission from [25]. Copyright 2011 Wiley-VCH.

With their LSPRs tuned to the proper wavelength, the strong absorption of AuNCs has been harnessed for diverse theranostic applications, including optical imaging, controlled release, and drug delivery. In one study, AuNCs were used to actively target subcutaneous tumor tissue in mice, leading to pronounced enhancement in PAT imaging [26]. Specifically, the surface of the nanocages was conjugated with poly(ethylene glycol) (PEG) chains terminated in [Nle⁴, d-Phe⁷]- α -melanocyte-stimulating hormone ([Nle⁴, d-Phe⁷]- α -MSH)—a peptide capable of binding to receptors on melanoma cells (Figure 4a). After intravenous injection of [Nle⁴, d-Phe⁷]- α -MSH-AuNCs, PA images were recorded at 0, 3 and 6 h, respectively. The images in Figure 4b–d clearly indicate the gradual accumulation of the AuNCs inside the tumor to greatly enhance the PA signal.

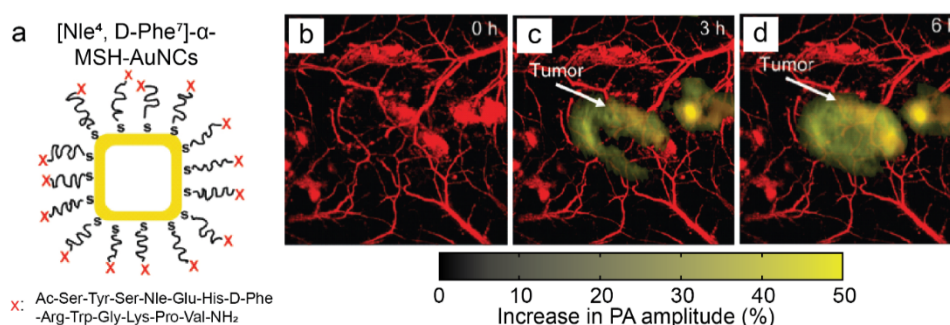


Figure 4. Use of Au nanocage as a contrast agent for photoacoustic (PA) imaging. (a) Schematic of the [Nle⁴,d-Phe⁷]- α -MSH-AuNCs. MSH: Melanocyte Stimulating Hormone. (b–d) PA images of the melanoma tissue

recorded at different time points (0, 3, and 6 h) post injection of [Nle4,d-Phe7]- α -MSH-AuNCs, with yellow and red corresponding to the melanoma and the surrounding vasculature. Reproduced with permission from [26]. Copyright 2010 American Science Society.

The strong NIR absorption of AuNCs also facilitates photothermal conversion for application in stimuli-triggered release. To this end, control can be achieved through two methods: either attaching gating polymer brushes to the surface of the AuNCs or filling the interior with a phase-change material (PCM), a substance that undergoes solid-to-liquid phase transition upon melting. In one approach, our group employed poly(*N*-isopropylacrylamide) (pNIPAAm)—a thermal-responsive polymer—to seal the pores on AuNCs [27]. As the local temperature increases due to the photothermal heating enabled by AuNCs, the polymer chains contract to allow the payloads to freely diffuse out through the pores. In another approach, our group loaded the cavity of the AuNCs with a PCM based on lauric acid. For the treatment of hypoxic cancer, 2,2'-azobis[2-(2-imidazolin-2-yl)propane] dihydrochloride (AIPH) was added into the PCM to generate AIPH-PCM-AuNCs (Figure 5a) [28]. Upon exposure to an NIR laser, the AuNCs were heated up to melt the PCM, simultaneously triggering the release and decomposition of AIPH. The free radicals derived from the decomposition of AIPH resulted in tumor cell apoptosis. As shown in Figure 5b, the amount of AIPH released is positively correlated with the intensity and duration of the laser. Furthermore, AIPH-induced reactive oxygen species (ROS) can be detected in A549 cancer cells through 2',7'-dichlorodihydrofluorescein diacetate (DCFHDA) staining even under tumor hypoxia conditions (Figure 5c).

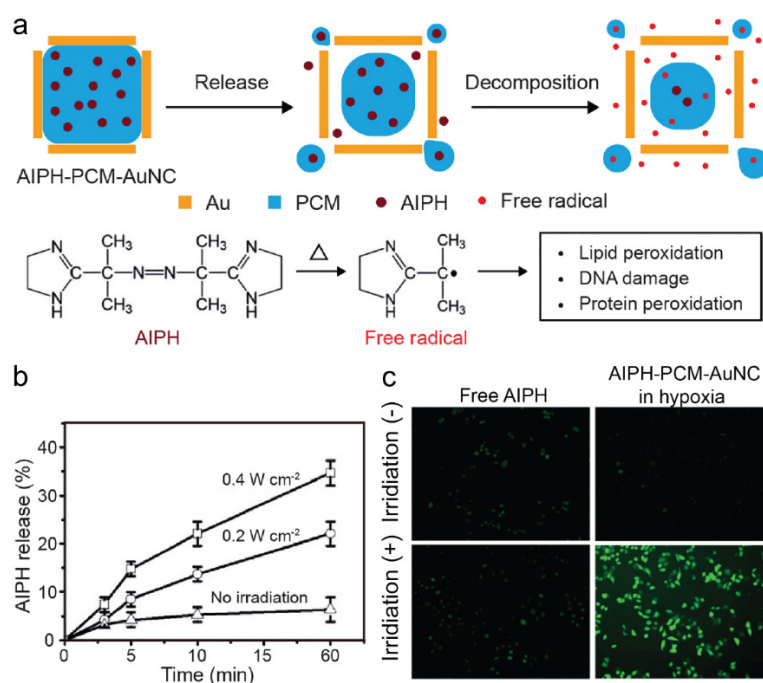


Figure 5. Use of Au nanocages for controlling the release of a therapeutic agent. **(a)** Schematic illustrating the controlled release of AIPH from the PCM loaded in the interior of Au nanocages upon laser irradiation. **(b)** Release profiles of AIPH upon laser irradiation at different irradiances. **(c)** Detection of AIPH-induced ROS in A549 cells by DCFHDA after laser irradiation for 30 min. **(a)** Reproduced with permission from [18]. Copyright 2020 the Royal Society of Chemistry. **(b–c)** Reproduced with permission from [28]. Copyright 2017 Wiley-VCH.

Silver is a common element used in biomedical applications. The antimicrobial activity of AgNPs has been extensively investigated. It is well-established that the nanoparticles could serve as effective growth inhibitors for various microorganisms, rendering them suitable for a range of medical devices and antimicrobial control systems. One study investigated AgNPs ranging from 5–25 nm in size while being supported on graphene oxide sheets, as confirmed by X-ray diffraction and electron microscopy [29]. The AgNPs effectively combat Gram-negative bacteria, with their effectiveness linked to their size and shape, showing promise for use in antimicrobial applications. As a relatively new modality, SERS imaging has benefited from AgNPs in biomedical applications such as the detection of specific biomarkers on cell surfaces for cancer diagnosis or tracking drug delivery [30]. Upon irradiation of AgNPs with a laser, enhanced electromagnetic fields are created in the vicinity of the nanoparticles to increase the Raman scattering cross-sections of molecules adsorbed on or near the nanoparticles, enabling highly sensitive detection through the fingerprinting of vibrational modes.

Among the radionuclides used for nanoparticle-based positron emission tomography (PET), ^{64}Cu occupies a unique position as it can be directly incorporated into Au nanocrystals through co-deposition, enabling precise control of radioactivity [31]. In one study, ^{64}Cu -doped AuNCs have been developed to enable image-guided therapy by combining the long half-life of ^{64}Cu for PET and the strong absorption of Au nanostructures in the NIR region for photothermal therapy. In a cancer mice model, both tumor targeting and PET imaging contrast enhancement were demonstrated, highlighting the potential of this unique class of Au-Cu alloy nanostructures for preclinical and translational applications (Figure 6) [32].

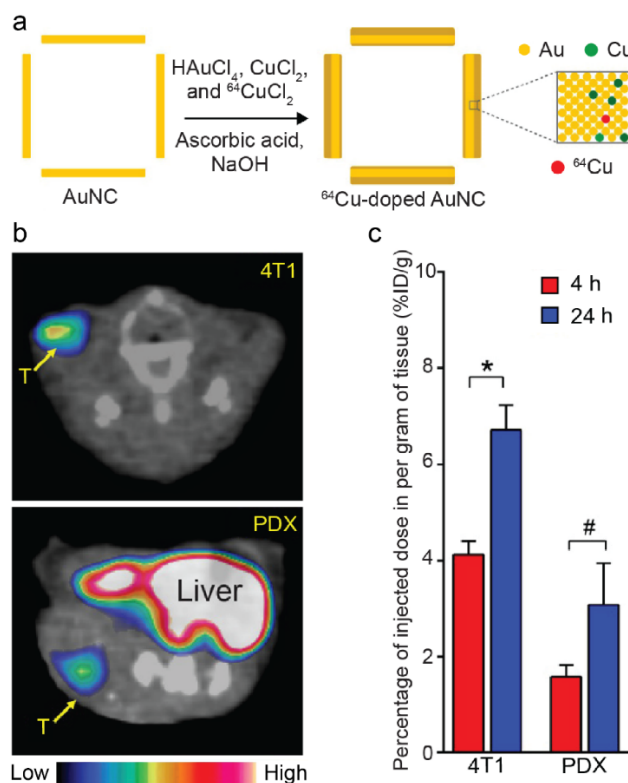


Figure 6. Use of ^{64}Cu -doped Au nanocages for PET. (a) Schematic illustrating the synthesis of ^{64}Cu -doped Au nanocages through co-deposition of Au, Cu, and ^{64}Cu atoms onto the walls of Au nanocages. (b) Transverse PET/CT images of the PEGylated, ^{64}Cu -doped Au nanocages in mice 4T1 and PDX tumor models recorded 24 h after injection. (c) Quantification of tumor uptake in both models, demonstrating effective accumulation of the nanocrystals at the tumor site. * $p < 0.0005$, # $p < 0.005$. Reproduced with permission from [32]. Copyright 2016 Wiley-VCH.

Due to the large atomic number, Ir nanocrystals have found use as a contrast agent for X-ray-based imaging and as an enhancer for radiotherapy. Small Ir nanoparticles (IrNPs) can be prepared using an aqueous method by reducing IrCl_3 with NaBH_4 without involving any surfactant or capping agent [33]. The as-obtained nanoparticles have promising potential for medical applications involving X-ray radiation. In vitro tests using Alamar Blue assay with liver and immune cells suggested that the IrNPs could be used safely in living organisms at concentrations of up to $100 \mu\text{M}$.

In a set of studies, Pt-nanocluster assemblies (PtNAs) comprising a pH-sensitive polymer (octadecylamine- $p(\text{API-Asp})_{10}$) and a liver cancer cell-targeting peptide have been demonstrated to successfully combat drug resistance and stem-like properties in liver cancer [34]. Significant death of liver cancer cells and the overcoming of chemotherapy medication resistance were achieved by PtNAs via the induction of DNA damage. The mechanism of these effects at the molecular level has also been investigated, suggesting that PtNAs hold promise for clinical treatment through the downregulation of highly expressed genes in liver cancer patients.

4. Conclusions and Outlook

The past two decades have witnessed remarkable advancement in the controlled synthesis of noble-metal nanocrystals, particularly Au and Ag, enabling precise manipulation of their sizes and morphologies. With their unique physiochemical properties and tunable architecture, engineered noble-metal nanostructures now serve as versatile tools in biomedical applications, supporting advanced bioimaging, stimuli-responsive drug delivery, and

antimicrobial or anticancer therapies. Despite this progress, challenges remain in improving synthesis scalability and investigating their long-term biocompatibility for successful clinical translation. By addressing the current limitations and exploring new research avenues, we can fully realize the immense promises noble-metal nanocrystals hold for improving diagnostics and therapies.

Author Contributions: Y.C.: visualization, writing—original draft, writing—reviewing and editing; E.Y.: writing—original draft, writing—reviewing and editing; Y.X.: conceptualization, writing—reviewing and editing. All authors have read and agreed to the published version of the manuscript.

Funding: The preparation of this manuscript was supported in part by startup funds from the Georgia Institute of Technology.

Conflicts of Interest: The authors declare no conflict of interest.

References

1. Cho, E.C.; Glaus, C.; Chen, J.; Welch, M.J.; Xia, Y. Inorganic Nanoparticle-Based Contrast Agents for Molecular Imaging. *Trends Mol. Med.* **2010**, *16*, 561–573. <https://doi.org/10.1016/j.molmed.2010.09.004>.
2. Yang, X.; Yang, M.; Pang, B.; Vara, M.; Xia, Y. Gold Nanomaterials at Work in Biomedicine. *Chem. Rev.* **2015**, *115*, 10410–10488. <https://doi.org/10.1021/acs.chemrev.5b00193>.
3. Xia, Y.; Xiong, Y.; Lim, B.; Skrabalak, S.E. Shape-Controlled Synthesis of Metal Nanocrystals: Simple Chemistry Meets Complex Physics? *Angew. Chem., Int. Ed.* **2009**, *48*, 60–103. <https://doi.org/10.1002/anie.200802248>.
4. Nguyen, Q.N.; Wang, C.; Shang, Y.; Janssen, A.; Xia, Y. Colloidal Synthesis of Metal Nanocrystals: From Asymmetrical Growth to Symmetry Breaking. *Chem. Rev.* **2022**, *123*, 3693–3760. <https://doi.org/10.1021/acs.chemrev.2c00468>.
5. Ji, X.; Song, X.; Li, J.; Bai, Y.; Yang, W.; Peng, X. Size Control of Gold Nanocrystals in Citrate Reduction: The Third Role of Citrate. *J. Am. Chem. Soc.* **2007**, *129*, 13939–13948. <https://doi.org/10.1021/ja074447k>.
6. Zheng, Y.; Ma, Y.; Zeng, J.; Zhong, X.; Jin, M.; Li, Z.-Y.; Xia, Y. Seed-Mediated Synthesis of Single-Crystal Gold Nanospheres with Controlled Diameters in the Range 5–30 nm and their Self-Assembly upon Dilution. *Chem. Asian J.* **2013**, *8*, 792–799. <https://doi.org/10.1002/asia.201201105>.
7. Zheng, Y.; Zhong, X.; Li, Z.; Xia, Y. Successive, Seed-Mediated Growth for the Synthesis of Single-Crystal Gold Nanospheres with Uniform Diameters Controlled in the Range of 5–150 nm. *Part. Part. Syst. Charact.* **2014**, *31*, 266–273. <https://doi.org/10.1002/ppsc.201300256>.
8. Huo, D.; Kim, M.J.; Lyu, Z.; Shi, Y.; Wiley, B.J.; Xia, Y. One-Dimensional Metal Nanostructures: From Colloidal Syntheses to Applications. *Chem. Rev.* **2019**, *119*, 8972–9073. <https://doi.org/10.1021/acs.chemrev.8b00745>.
9. Wang, Y.; Zheng, Y.; Huang, C.Z.; Xia, Y. Synthesis of Ag Nanocubes 18–32 nm in Edge Length: The Effects of Polyol on Reduction Kinetics, Size Control, and Reproducibility. *J. Am. Chem. Soc.* **2013**, *135*, 1941–1951. <https://doi.org/10.1021/ja311503q>.
10. Sun, Y.; Xia, Y. Shape-Controlled Synthesis of Gold and Silver Nanoparticles. *Science* **2002**, *298*, 2176–2179. <https://doi.org/10.1126/science.1077229>.
11. Zhang, Q.; Li, W.; Wen, L.-P.; Chen, J.; Xia, Y. Facile Synthesis of Ag Nanocubes of 30 to 70 nm in Edge Length with CF₃COOAg as a Precursor. *Chem. Eur. J.* **2010**, *16*, 10234–10239. <https://doi.org/10.1002/chem.201000341>.
12. Siekkinen, A.R.; McLellan, J.M.; Chen, J.; Xia, Y. Rapid Synthesis of Small Silver Nanocubes by Mediating Polyol Reduction with a Trace Amount of Sodium Sulfide or Sodium Hydrosulfide. *Chem. Phys. Lett.* **2006**, *432*, 491–496. <https://doi.org/10.1016/j.cplett.2006.10.095>.
13. Wiley, B.; Herricks, T.; Sun, Y.; Xia, Y. Polyol Synthesis of Silver Nanoparticles: Use of Chloride and Oxygen to Promote the Formation of Single-Crystal, Truncated Cubes and Tetrahedrons. *Nano Lett.* **2004**, *4*, 1733–1739. <https://doi.org/10.1021/nl048912c>.
14. Lyu, Z.; Shang, Y.; Xia, Y. Shape-Controlled Synthesis of Copper Nanocrystals for Plasmonic, Biomedical, and Electrocatalytic Applications. *Acc. Mater. Res.* **2022**, *3*, 1137–1148. <https://doi.org/10.1021/accountsmr.2c00134>.
15. Lyu, Z.; Xie, M.; Aldama, E.; Zhao, M.; Qiu, J.; Zhou, S.; Xia, Y. Au@Cu Core–Shell Nanocubes with Controllable Sizes in the Range of 20–30 nm for Applications in Catalysis and Plasmonics. *ACS Appl. Nano Mater.* **2019**, *2*, 1533–1540. <https://doi.org/10.1021/acsanm.9b00016>.
16. Mayer, M.; Scarabelli, L.; March, K.; Altantzis, T.; Tebbe, M.; Kociak, M.; Bals, S.; Garcia de Abajo, F.J.; Fery, A.; Liz-Marzan, L.M. Controlled Living Nanowire Growth: Precise Control over the Morphology and Optical Properties of AgAuAg Bimetallic Nanowires. *Nano Lett.* **2015**, *15*, 5427–5437. <https://doi.org/10.1021/acs.nanolett.5b01833>.
17. Yang, M.; Wang, W.; Qiu, J.; Bai, M.-Y.; Xia, Y. Direct Visualization and Semi-Quantitative Analysis of Payload Loading in the Case of Gold Nanocages. *Angew. Chem., Int. Ed.* **2019**, *58*, 17671–17674. <https://doi.org/10.1002/anie.201911163>.
18. Qiu, J.; Xie, M.; Wu, T.; Qin, D.; Xia, Y. Gold Nanocages for Effective Photothermal Conversion and Related Applications. *Chem. Sci.* **2020**, *11*, 12955–12973. <https://doi.org/10.1039/D0SC05146B>.

19. Mieszawska, A.J.; Mulder, W.J.; Fayad, Z.A.; Cormode, D.P. Multifunctional Gold Nanoparticles for Diagnosis and Therapy of Disease. *Mol. Pharmaceutics* **2013**, *10*, 831–847. <https://doi.org/10.1021/mp3005885>.
20. Gnath, C.; Johnson, S. Strips of Hope: Accuracy of Home Pregnancy Tests and New Developments. *Geburtshilfe Frauenheilkd.* **2014**, *74*, 661–669. <https://doi.org/10.1055/s-0034-1368589>.
21. Wikipedia: Pregnancy Test. Available online: https://en.wikipedia.org/wiki/Pregnancy_test#/media/File:Pregnancy_Test_Positive.jpg (accessed on 22 February 2025).
22. Moitra, P.; Alafeef, M.; Dighe, K.; Frieman, M.B.; Pan, D. Selective Naked-Eye Detection of SARS-CoV-2 Mediated by N Gene Targeted Antisense Oligonucleotide Capped Plasmonic Nanoparticles. *ACS Nano* **2020**, *14*, 7617–7627. <https://doi.org/10.1021/acsnano.0c03822>.
23. Cobley, C.M.; Chen, J.; Cho, E.C.; Wang, L.V.; Xia, Y. Gold nanostructures: a class of multifunctional materials for biomedical applications. *Chem. Soc. Rev.* **2011**, *40*, 44–56. <https://doi.org/10.1039/B821763G>.
24. Hu, M.; Chen, J.; Li, Z.-Y.; Au, L.; Hartland, G.V.; Li, X.; Marquez, M.; Xia, Y. Gold Nanostructures: Engineering Their Plasmonic Properties for Biomedical Applications. *Chem. Soc. Rev.* **2006**, *35*, 1084–1094. <https://doi.org/10.1039/b517615h>.
25. Li, W.; Brown, P.K.; Wang, L.V.; Xia, Y. Gold Nanocages as Contrast Agents for Photoacoustic Imaging. *Contrast Media Mol. Imaging* **2011**, *6*, 370–377. <https://doi.org/10.1002/cmimi.439>
26. Kim, C.; Cho, E.C.; Chen, J.; Song, K.H.; Au, L.; Favazza, C.; Zhang, Q.; Cobley, C.M.; Gao, F.; Xia, Y. In Vivo Molecular Photoacoustic Tomography of Melanomas Targeted by Bioconjugated Gold Nanocages. *ACS Nano* **2010**, *4*, 4559–4564. <https://doi.org/10.1021/nn100736c>.
27. Yavuz, M.S.; Cheng, Y.; Chen, J.; Cobley, C.M.; Zhang, Q.; Rycenga, M.; Xie, J.; Kim, C.; Song, K.H.; Schwartz, A.G.; et al. Gold Nanocages Covered by Smart Polymers for Controlled Release with Near-Infrared Light. *Nat. Mater.* **2009**, *8*, 935–939. <https://doi.org/10.1038/nmat2564>.
28. Shen, S.; Zhu, C.; Huo, D.; Yang, M.; Xue, J.; Xia, Y. A Hybrid Nanomaterial for the Controlled Generation of Free Radicals and Oxidative Destruction of Hypoxic Cancer Cells. *Angew. Chem., Int. Ed.* **2017**, *56*, 8801–8804. <https://doi.org/10.1002/anie.201702898>.
29. Das, M.R.; Sarma, R.K.; Saikia, R.; Kale, V.S.; Shelke, M.V.; Sengupta, P. Synthesis of Silver Nanoparticles in an Aqueous Suspension of Graphene Oxide Sheets and Its Antimicrobial Activity. *Colloids Surf. B* **2011**, *83*, 16–22. <https://doi.org/10.1016/j.colsurfb.2010.10.033>.
30. Schlücker, S. SERS Microscopy: Nanoparticle Probes and Biomedical Applications. *ChemPhysChem* **2009**, *10*, 1344–1354. <https://doi.org/10.1002/cphc.200900119>.
31. Zhao, Y.; Sultan, D.; Detering, L.; Cho, S.; Sun, G.; Pierce, R.; Wooley, K.L.; Liu, Y. Copper-64-Alloyed Gold Nanoparticles for Cancer Imaging: Improved Radiolabel Stability and Diagnostic Accuracy. *Angew. Chem. Int. Ed.* **2013**, *53*, 156–159. <https://doi.org/10.1002/ange.201308494>.
32. Yang, M.; Huo, D.; Gilroy, K.D.; Sun, X.; Sultan, D.; Luehmann, H.; Detering, L.; Li, S.; Qin, D.; Liu, Y.; et al. Facile Synthesis of ⁶⁴Cu-Doped Au Nanocages for Positron Emission Tomography Imaging. *ChemNanoMat* **2017**, *3*, 44–50. <https://doi.org/10.1002/cnma.201600281>.
33. Brown, A.L.; Winter, H.; Goforth, A.M.; Sahay, G.; Sun, C. Facile Synthesis of Ligand-Free Iridium Nanoparticles and Their In Vitro Biocompatibility. *Nanoscale Res. Lett.* **2018**, *13*, 1–6. <https://doi.org/10.1186/s11671-018-2621-3>.
34. Xia, H.; Li, F.; Hu, X.; Park, W.; Wang, S.; Jang, Y.; Du, Y.; Baik, S.; Cho, S.; Kang, T. pH-Sensitive Pt Nanocluster Assembly Overcomes Cisplatin Resistance and Heterogeneous Stemness of Hepatocellular Carcinoma. *ACS Cent. Sci.* **2016**, *2*, 802–811. <https://doi.org/10.1021/acscentsci.6b00197>.